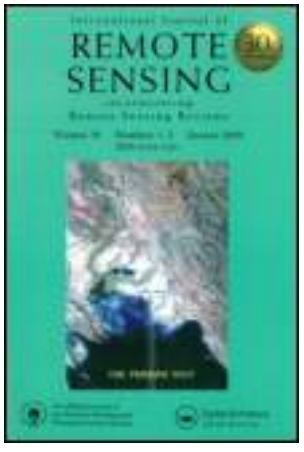

International Journal of Remote Sensing

Publication details, including instructions for authors and subscription information:
http://www.tandfonline.com/loi/tres20

Large-scale leaf area index inversion algorithms from high-resolution airborne imagery

Alemu Gonsamo [a], P. Pellikka [a] & D. J. King [b]

[a] Department of Geography, University of Helsinki, PO Box 64, FIN-00014, Helsinki, Finland

[b] Department of Geography and Environmental Studies, Carleton University, 1125 Colonel By Drive, Ottawa, ON, Canada, K1S 5B6

Available online: 30 Jun 2011

To cite this article: Alemu Gonsamo, P. Pellikka & D. J. King (2011): Large-scale leaf area index inversion algorithms from high-resolution airborne imagery, International Journal of Remote Sensing, 32:14, 3897-3916

To link to this article: http://dx.doi.org/10.1080/01431161003801302

International Journal of Remote Sensing
Vol. 32, No. 14, 20 July 2011, 3897–3916

Taylor & Francis
Taylor & Francis Group

Large-scale leaf area index inversion algorithms from high-resolution airborne imagery

ALEMU GONSAMO*†, P. PELLIKKA† and D. J. KING‡
†Department of Geography, University of Helsinki, PO Box 64, FIN-00014 Helsinki, Finland
‡Department of Geography and Environmental Studies, Carleton University, 1125 Colonel By Drive, Ottawa, ON, Canada, K1S 5B6

(*Received 10 June 2008; in final form 11 February 2010*)

Large-scale leaf area index (LAI) inversion algorithms were developed to determine the LAI of a forest located in Gatineau Park, Canada, using high-resolution colour and colour infrared (CIR) digital airborne imagery. The algorithms are parameter-independent and developed based on the principles of optical field instruments for gap fraction measurements. Cloud-free colour and CIR images were acquired on 21 August 2007 with 35 and 60 cm nominal ground pixel size, respectively. Normalized Difference Vegetation Index (NDVI), maximum likelihood and object-oriented classifications, and principal component analysis (PCA) methods were applied to calculate the mono-directional gap fraction. Subsequently, LAI was derived from inversion and compared with ground measurements made in 54 plots of 20 by 20 m using hemispherical photography between 10 and 20 August 2007. There was high inter-correlation (the Pearson correlation coefficient, $R > 0.5$, $p < 0.01$) among LAI values inverted using the classifications and PCA methods, but neither were highly correlated with LAI inverted from the NDVI method. LAI inverted from the NDVI-based gap fraction significantly correlated with ground-measured LAI ($R = 0.63$, root mean square error (RMSE) = 0.52), while LAI inverted from the classification and PCA-derived gap fraction showed poor correlation with ground-measured LAI. Consequently, the NDVI method was used to invert LAI for the whole study area and produce a 20-m resolution LAI map.

1. Introduction

Vegetation plays a major role in global physical and biogeochemical processes and strongly regulates regional and global climate. This role is primarily based on a simple structural unit: the leaf. The number and photosynthetic capacity of leaves in a forest control primary productivity, climate, water and carbon gas exchanges and radiation extinction and are, therefore, key components of physiological, climatological and biogeochemical processes in ecosystems. Extensive work has been conducted on the analysis of ecosystem process and properties using a single measure of canopy structure, that is leaf area index (LAI) (Asner *et al*. 2003). LAI was first defined by Watson (1947) as the total one-sided area of photosynthetic tissue per unit surface area. In the current literature, LAI is defined as one-half of the total leaf area per unit

*Corresponding author. Email: alemu.gonsamo@helsinki.fi

International Journal of Remote Sensing
ISSN 0143-1161 print/ISSN 1366-5901 online
http://www.tandf.co.uk/journals
DOI: 10.1080/01431161003801302

ground surface area projected on the local horizontal datum (Leblanc *et al.* 2005, Gonsamo and Pellikka 2008). As both leaf and ground areas are normally measured in the same units (m^2), LAI is dimensionless and can be analysed across a range of spatial scales.

LAI can be determined *in situ* or using remote sensing techniques. *In situ* determination is conducted directly by area harvest and litter-fall collection or indirectly using optical field instruments which measure the light transmission under the canopy (Jonckheere *et al.* 2004). Many optical field instruments and methods of measuring LAI have been developed in the last one and a half decades. Techniques based on gap-fraction analysis assume that LAI can be calculated from canopy transmittance (the fraction of direct solar radiation which penetrates the canopy) and are well reported in the literature (Jonckheere *et al.* 2004). Measurements of canopy transmittance using optical field instruments are based on light recorded at a point under the canopy. This technique can also be applied by observing the canopy from above, provided that high-spatial-resolution remote sensing imagery is available to distinguish shadows/gaps from canopy.

Remote sensing techniques use canopy radiance data to indirectly estimate LAI. They are the only alternative way to estimate LAI and its temporal variability at multiple scales because observations can be obtained over large areas with high revisitation frequency. Methods to estimate LAI from remote sensing data can be broadly categorized into two main classes: empirical methods based on the relationships between LAI and vegetation indices or other image-derived measures; and physical models based on canopy reflectance model inversion (Goel 1988, Turner *et al.* 1999, Gong *et al.* 2003, Berterretche *et al.* 2005). Both methods are parameter-dependent. Empirical methods are limited by effects of varying understorey and soil background reflectance as well as saturation of vegetation indices at high LAI values. Reflectance models are generally mathematically invertible; however, they do not provide a complete description of the actual radiative transfer and canopy structure. There are no perfect canopy reflectance models that can be directly used for LAI inversion over large areas. Furthermore, selection of the parameters for the inversion of canopy reflectance models is complicated, and some parameters are very difficult to determine. An estimated reflectance value in a pixel often has large relative uncertainty and the inverse solution is not always unique as different sets of physical variables may yield very similar spectral signatures. For common usage of remotely sensed data, users will generally avoid complex models. The success of LAI estimation from remotely sensed data remains, however, cumbersome and there is always a need to calibrate remotely retrieved parameters with *in situ* observation. In addition to the most commonly used empirical methods of LAI estimation from remote sensing, studies have effectively employed parameter-independent LAI inversion algorithms based on gap fraction/fractional vegetation cover derived from satellite data (Sprintsin *et al.* 2007).

A number of studies successfully estimated gap fraction or fractional canopy cover from satellite remote sensing using the Normalized Difference Vegetation Index (NDVI) (Richardson and Wiegand 1977, Gutman and Ignatov 1998, Carpenter *et al.* 1999, Xiao and Moody 2005, Sprintsin *et al.* 2007). However, the use of NDVI for gap extraction is limited by the often coarse resolution of satellite observations, which results in mixed pixels made up of more than one land cover type. By using high-resolution aerial imagery, relatively 'pure' small pixels of canopy, shadow and soil/litter can be obtained. Several studies have also applied spectral unmixing (Hu *et al.* 2004) and textural analysis (Wulder *et al.* 1996, 1998) to retrieve LAI from

airborne imagery. The objective of this study was to evaluate and compare the potential of four parameter-independent LAI inversion algorithms applied to colour and colour infrared (CIR) airborne imagery. The various procedures are validated using ground LAI measurements.

2. Material and methods

2.1 *Site description*

The study site is located in the Great Lakes, St Lawrence Forest in southern Quebec, Canada. It is part of the Gatineau Park (figure 1), which is managed by the National Capital Commission (NCC) of Canada and centred at 45° 30′ N, 75° 52′ W. The park is about 10 by 50 km and is mostly temperate hardwood forest with a dominant overstorey of sugar maple (*Acer saccharum* Marsh.) and small patches dominated by American beech (*Fagus grandifolia* Ehrh.), trembling aspen (*Populus tremuloides* Michx.) and red oak (*Quercus rubra* L.). Small numbers of red maple (*Acer rubrum* L.), American basswood (*Tilia americana* L.), ironwood (*Ostrya virginiana* (Mill.) K. Koch), white ash (*Fraxinus americana* L.), black ash (*Fraxinus nigra* Marsh.), white birch (*Betula papyrifera* Marsh.) and black cherry (*Prunus serotina* Ehrh.) are also present. The study plots were located in the southern portion of the park (figure 1). They have been part of ongoing research on monitoring forest damage, structure, health and succession following the ice storm of 1998 (Pellikka *et al*. 2000b, King *et al*. 2005).

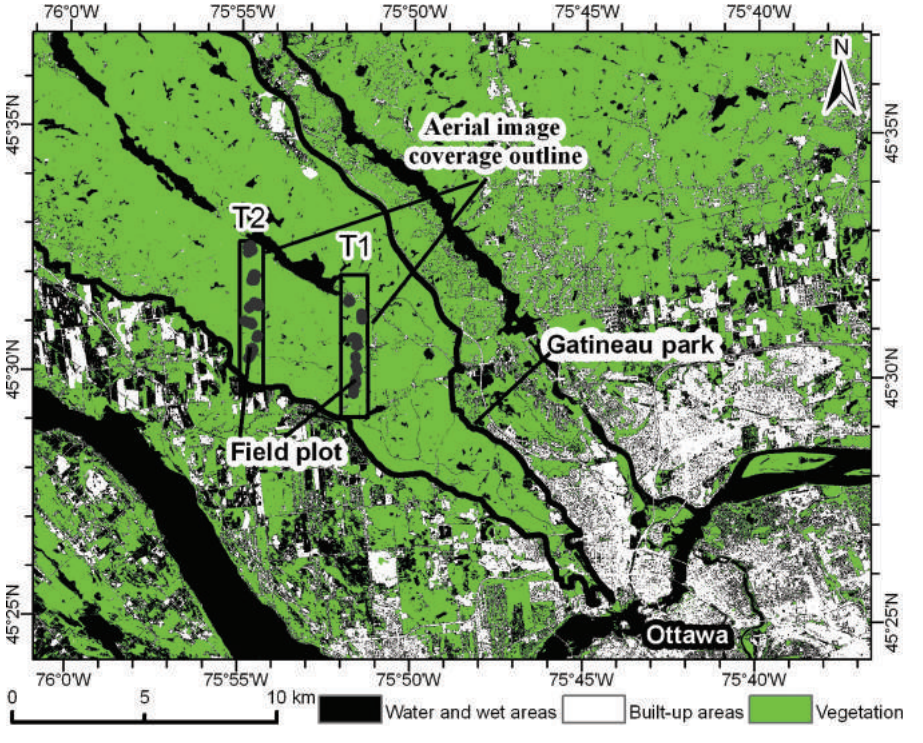

Figure 1. General land cover map showing the portion of Gatineau Park, outline of aerial image coverage and field plot locations of transect one (T1) and two (T2).

2.2 *Study plots and LAI measurement*

In 1998, 61 plots, each 20 by 20 m, were placed on two north–south oriented transects (figure 1) in the Gatineau Park for the ice storm damage studies (Pellikka *et al*. 2000b). This study is a continuation of that research so the same transects and plots were used to collect field LAI measurements. Fifty-four of these plots that could be easily found in 2007 were selected. Plot corners were surveyed using differential Global Positioning System (GPS) to provide positional accuracy on the order of <1 m (Pellikka *et al*. 2000b). This level of accuracy is critical for airborne remote sensing, where image pixel sizes are small.

The ground LAI measurements were collected using digital hemispherical photography between 10 and 20 August 2007. The photographs were acquired using a high-resolution (8 mega pixels) Nikon Coolpix 8800 VR digital camera equipped with a fish-eye Nikon FC-E9 lens adapter (Nikon Inc., Japan). In total, five photographs were acquired in each study plot, one at each corner and one at the centre. The measurements were performed using manual exposure under uniformly overcast conditions to minimize the anisotropy of the sky radiance and to reduce the scattering fluxes in the digital image. The camera was mounted and levelled on a tripod at a height of 1.3 m above the ground. The LAI was computed for the range of 0–60° view zenith angle to reduce the growing effects of mixed pixels near the horizon, which result from light scattering and coarse resolution. All photographs were analysed using CAN_EYE software (e.g. Demarez *et al*. 2008). Fractional vegetation cover was extracted from the average gap fraction computed within 0–20° view zenith angle. (Note: for simplicity, the effective LAI, which assumes random foliage distribution, was used in this study and is hereafter referred to as LAI.)

2.3 *Airborne imagery acquisition and processing*

A data set of colour and CIR digital camera images was captured on a cloud-free day of 21 August 2007, between 12:32 and 13:24 local time, from an aircraft flying at approximately 309 m above ground level. During the acquisition, the solar zenith angle was between 34.3° and 33.6° and the azimuth angle was between 164° and 188.1°. The CIR camera was a Duncantech MS4100 with 1920 × 1080 pixel format and a 24 mm lens. It is a 3-CCD camera with dispersion optics that split incident irradiance into three bands: green (500–600 nm), red (600–700 nm) and near-infrared (NIR, 750–850 nm). The colour camera was a Nikon D200, a single CCD with 3872 × 2592 pixel format and a 28 mm focal length lens. Exposures were set before each flight line to optimize the dynamic range and to result in image motion during each exposure of less than half a pixel. Exposure intervals for both cameras were set to provide 60% forward overlap. The nominal ground pixel size was 60 cm for the CIR data and 35 cm for the colour data.

The images were georectified using 25 cm pixel orthophotos provided by the NCC. An average of 10 ground control points (GCPs) was selected for each image. A first-order polynomial and nearest neighbour interpolation were used as the warping and grey level resampling methods, respectively. The output projection for the registered images was UTM zone 18 with an NAD83 datum. Mosaics were assembled using pixels in the overlap area of each image pair that were closest to nadir. This minimized the effect of the bi-directional reflectance distribution function (BRDF), vignetting and light fall-off (Pellikka 1998, Lévesque and King 1999, Pellikka *et al*. 2000a). The mosaics were also clipped from each side to restrict the across-track view

angle to 8°. The ground plots were distributed along the centre of the mosaic (flight line) so the between-plot optical variation was minimized.

2.4 *Estimation of vegetation fractional cover*

A number of studies have successfully derived fractional cover of vegetation from remote sensing observations (Richardson and Wiegand 1977, Carpenter *et al.* 1999, Xiao and Moody 2005, Sprintsin *et al.* 2007). Fractional cover (f_c) is the percentage of vegetative cover projected vertically onto the ground. In the context of a remotely sensed image, the f_c values represent the percentage of vegetative cover present in each pixel or in a unit area. Fractional cover is used in the retrieval of canopy LAI from remotely sensed imagery as described in section 2.5. To estimate f_c, four procedures were implemented and compared, namely a scaled NDVI technique, maximum likelihood and object-oriented classifications, and principal component analysis (PCA).

2.4.1 Extraction of fractional cover from NDVI. The most common method to estimate fractional cover from a vegetation index uses NDVI and was proposed by Gutman and Ignatov (1998). NDVI of a pixel is a weighted sum of vegetation NDVI ($NDVI_g$) and non-vegetation NDVI ($NDVI_{back}$):

$$NDVI = f_c(NDVI_g) + (1 - f_c)(NDVI_{back}). \quad (1)$$

Rearranging equation (1) yields:

$$f_c = \frac{(NDVI) - (NDVI_{back})}{(NDVI_g) - (NDVI_{back})}, \quad (2)$$

where $NDVI_g$ is the maximum or saturated NDVI, which is defined as the NDVI where vegetation occupies the full field of view, and $NDVI_{back}$ is the minimum or background NDVI. A common approach to the retrieval of background and saturated NDVI values is through time series analysis. However, leaf optical properties can vary during the year independently of LAI. It may be difficult to determine $NDVI_{back}$ because pixels may present partial or full soil cover, but this problem is less significant with high-resolution remote sensing imagery. Owing to the well-documented nature of NDVI saturation above a given LAI threshold (e.g. about LAI = 2–3; Sellers *et al.* 1986), $NDVI_g$ may be relatively constant in dense forests with varying LAI. It is also common to have $NDVI_{back}$ values below 0, as the NIR reflectance of water can be less than red reflectance. Leblanc *et al.* (1997) reported that, for the same canopy, the saturation and background NDVI values vary less than 20% with view and illumination angles except for a small angular range near the hotspot. Theoretically, for each canopy type and each solar and view angle configuration, there should be one pair of saturated and background NDVI values.

To determine the saturated and background NDVI, the frequency distribution of computed NDVI for each image mosaic was calculated separately and combined into one histogram. The NDVI values at the 1% cut-off bounds (1st and 99th percentiles) in the histogram were taken as background and saturated NDVI values. Other studies have used the 90th percentile as $NDVI_g$ because NDVI increases with increasing view angle due to the effect of multiple scattering (Tang *et al.* 2007). However, in this study, with narrow view angles and high spatial resolution, the 99th percentile was deemed to be reliable in representing saturated NDVI. As illustrated in equation (2), the background NDVI has little influence on the accuracy of LAI inversion.

The minimum NDVI values for transect one (T1) and two (T2) (figure 1) were –0.60 and –0.61, respectively, and the maxima were 0.89 and 0.93, respectively. Consequently, the background and saturated NDVI computed from the 1% cut-off bounds were 0.01 and 0.79, respectively, for T1 and 0.16 and 0.81, respectively, for T2. When both transect NDVI histograms were combined, the background and saturated NDVI were 0.08 and 0.80, respectively. The individual transect and combined transect values were each tested in the estimation of fractional vegetation cover (equation (2)) and subsequently LAI. In addition, evaluation was conducted of background and saturated NDVI computed from each plot subscene.

2.4.2 Extraction of fractional cover from land cover classification. Image classification was conducted on both the true colour and CIR mosaics. It was assumed that the imagery was not affected by BRDF, vignetting and light fall-off, since the plots were situated along the flight line centre and only the areas closest to nadir of each scene were mosaicked. The training sites were selected visually from the scene and both sets of imagery were classified into five classes (canopy, water, road, soil and gap) using the conventional supervised maximum likelihood classification procedure. The selected pixels of training sites (an average per class of 76 173 pixels for the colour imagery and 42 357 pixels for the CIR imagery) were evaluated for class separability using transformed divergence (TD; Jensen 1996). The average TD distances of the five classes were above 1900 for both the colour and CIR mosaics. A binary map of canopy and non-canopy was produced by combining non-canopy classes into a 'gap' class. Fractional cover was derived using the following equation for plot subscene and mapping grids:

$$f_c = \frac{p_c}{p_t}, \tag{3}$$

where p_c is the number of pixels recorded as canopy and p_t is the total number of pixels in a specific plot subscene.

Besides the above conventional pixel-based classification procedure, an object-oriented multi-resolution segmentation and classification process was implemented for both the colour and CIR mosaics using Definiens Professional version 5 software, previously known as eCognition (Definiens AG., Munich, Germany). Object-oriented image analysis has been shown to be an effective tool for classification of high-resolution remote sensing imagery (Herold *et al*. 2003, Laliberte *et al*. 2004). The initial step is the segmentation procedure or grouping of neighbouring pixels into homogeneous patches (i.e. image objects). The parameters that determine the output of the segmentation process are the spatial scale, colour/shape and smoothness/compactness, for which we adopted a scale factor of 10, a colour/shape factor of 0.9/0.1 and a smoothness/compactness factor of 0.5/0.5 for both image types based on trial and error to retrieve all small gaps. The object features used to classify the colour camera image objects were the mean, maximum, minimum and standard deviation of each band as well as the product of all three bands. For the CIR image objects the mean, maximum, minimum and standard deviation of each band as well as the simple ratio of NIR to red were used. Feature space optimization was conducted to select the pre-set image object features based on the maximum classification distance. Sample objects were selected for each class visually to extract training data for use with a nearest neighbour classifier, which assigned each object to the class of the nearest sample object (water, shadow, road, soil and canopy) in the feature space. As for the

pixel-based classification, the water, shadow, road and soil classes were combined to form a 'gap' class and a binary map of canopy and non-canopy was derived using equation (3).

2.4.3 Extraction of fractional cover from principal components analysis. Since there were high correlations among bands in the colour space, fractional vegetation cover was also extracted from uncorrelated principal components through a threshold technique. The first principal component represented almost all the data variance (minimum of 81%) and was used alone to distinguish pure gap or canopy pixels from mixed ones. The lowest brightness (DN_{min}) represented pure pixels of complete shadow and water, while the highest brightness (DN_{Emax}) represented pure pixels of soil, roads and artificial objects such as buildings. The brightness DN_{max} is a pixel value which separates the mixed and pure canopy pixels. The pixels between DN_{max} and DN_{Emax} represent pure pixels of canopy. For mixed pixels (between DN_{min} and DN_{max}), by assuming that the linear response of the CCD camera is represented by a linear brightness gradient in the first principal component, the within pixel vegetation fraction was estimated as:

$$\begin{aligned} f_c &= 0, && \text{for} \quad DN<DN_{min}; \\ f_c &= 0, && \text{for} \quad DN>DN_{Emax}; \\ f_c &= \frac{(DN)-(DN_{min})}{(DN_{max})-(DN_{min})}, && \text{for} \quad DN_{min}<DN<DN_{max}; \\ f_c &= 1, && \text{for} \quad DN_{max}<DN<DN_{Emax}; \end{aligned} \tag{4}$$

where DN is the digital number of a pixel. The thresholds DN_{min}, DN_{max} and DN_{Emax} were found visually by inspecting the entire mosaic. For the CIR imagery, the range of mixed pixels was 110 DN and for the colour image it was 190 DN. This means that the vegetation fraction resolution is at best 1/110 and 1/190 of the pixel size for the CIR and colour imagery, respectively. This level of sub-pixel vegetation/gap resolution may improve results within very dense canopies.

2.5 *Large-scale LAI inversion algorithm*

Theory shows that LAI can be estimated from the distribution of gap probability over the hemisphere (Jonckheere *et al.* 2004). Gap probability can be derived from the ratio of the above and below canopy radiation, which is commonly measured using ground-based methods. This is also valid when the canopy is observed from above, provided that vegetation and non-vegetation components are distinguishable (Tang *et al.* 2007). Such retrieval of LAI independently from *in situ* measurements requires high spatial resolution provided by airborne remote sensing. Assuming that the tree crowns are opaque and the only transmission is through the gaps in the canopy, the fraction of incident light transmitted through a canopy or mono-directional gap (P_o) can be described as:

$$P_o = 1 - f_c. \tag{5}$$

P_o can also be related to LAI using Beer–Lambert's law as:

$$P_o = \exp[-k(\mathrm{LAI})], \tag{6}$$

where k is defined following equation (10). Rearranging equations (5) and (6) yields:

$$1 - f_c = \exp[-k(\mathrm{LAI})]. \tag{7}$$

Therefore, for a known value of f_c and k, LAI can be calculated as:

$$\mathrm{LAI} = -\frac{\ln(1 - f_c)}{k}. \tag{8}$$

By combining equations (2) and (8), LAI can be estimated from NDVI as:

$$\mathrm{LAI} = -\frac{\ln\left(1 - \frac{(\mathrm{NDVI}) - (\mathrm{NDVI}_{\mathrm{back}})}{(\mathrm{NDVI}_g) - (\mathrm{NDVI}_{\mathrm{back}})}\right)}{k}. \tag{9}$$

Alternatively, by combining equations (3)–(5) with (8), LAI from two classification procedures and PCA can be estimated as:

$$\mathrm{LAI} = -\frac{\ln(P_o)}{k}, \tag{10}$$

where $k(k = G(\theta)/\cos\theta)$ is an empirically determined extinction coefficient, and G is the fraction of total foliage area that is perpendicular to the view zenith angle θ. For a broadleaved forest, k typically ranges between 0.42 and 0.58 (Bréda 2003; see summary of lists of different k values). In this study, k was assumed to be 0.5, which is a good approximation for a broadleaved forest considering the near-nadir view. Additionally, k, now called k_{aerial}, was determined using the hemispherical photograph measurement of LAI in order to invert equation (8) as follows:

$$k_{\mathrm{aerial}} = -\frac{\ln(1 - f_{\mathrm{c:aerial}}\mathrm{NDVI})}{(\mathrm{LAI}_{\mathrm{ground}})}, \tag{11}$$

where $f_{\mathrm{c:aerialNDVI}}$ is the fractional cover derived from NDVI analysis and $\mathrm{LAI}_{\mathrm{ground}}$ is the LAI estimated from hemispherical photography. The estimated k using equation (11) ranges from 0.4 to 0.6 with an average of 0.5, which is in good agreement with previous studies (Bréda 2003). Consequently, we used 0.5 as the k-value in all analysis cases.

2.6 *Statistical analysis and validation*

The aim of this research was to compare four parameter-independent methods for LAI extraction from both colour and CIR airborne imagery and not to develop an optimal model (i.e. one with the best fit possible). Each method was evaluated using LAI derived from the hemispherical photography. In order to do this, first each method was evaluated at the subscene scale, which covers only the ground plot area. The best method was then selected to predict LAI and produce a map for the whole data coverage.

The NDVI–f_c relationship is virtually scale-independent as long as very-high-resolution data is used, as demonstrated by Price (1990) and Jiang *et al.* (2007). The NDVI, land cover analysis and PCA were first computed at the pixel level or at the object level in the case of object-oriented segmentation. At the plot level, the subscene average was used to extract f_c and eventually inverted to LAI. In addition to this, inter-pixel variation within crowns caused by shading from canopy elements (leaves, branches) is addressed by considering only 'effective LAI', which directly contributes the canopy interception of the incident radiation. The subscene gap fraction extracted using all the three methods represents both between- and within-crown gaps.

At the subscene scale, before LAI extraction, the question of whether the 20 by 20 m plot size adequately represented the spatial variability of fractional vegetation cover was analysed. There could also be a possibility of image georeferencing error that could result in image data being extracted for calculation of f_c that were in a different location from the ground plots. Grids of 20 by 20 m to 50 by 50 m in 10 m intervals were placed over the entire image scene and f_c was determined using the four methods. No significant differences were found at the different spatial extents and the best fit to the ground measurement of f_c was found to be at the 20 m extent. Thus, in subsequent LAI mapping with the best of the four algorithms, the 20 by 20 m grid was used in a north–south orientation (the same as ground plot orientation) and the gap fraction was computed and inverted for each cell.

Three measures were used to evaluate algorithm effectiveness:

(1) the Pearson correlation coefficient (R) between measured and estimated LAI;
(2) the root mean square error (RMSE) of LAI estimation; and
(3) LAI estimation accuracy based on the overall average accuracy (OAA), defined as

$$\mathrm{OAA}(\%) = \left[1 - \frac{(\mathrm{RSD})}{y_{\mathrm{mean}}}\right] 100, \tag{12}$$

where

$$\text{residual standard deviation } (\mathrm{RSD}) = \sqrt{\frac{\sum_{i=1}^{n} (y_i - y_j)^2}{n-1}}; \quad y_{\mathrm{mean}} = \frac{\sum_{i=n}^{n} y_i}{n};$$

$y_i (i = 1, 2, 3, \ldots, n)$ are ground LAI measurements; y_j are the corresponding predicted LAI values; and n is the number of samples.

In addition, visual examination of LAI maps was conducted in comparison with the CIR image to assess the overall spatial distribution of predicted LAI.

3. Results

The classifications (maximum likelihood and object-oriented) and the PCA algorithm for fractional vegetation cover extraction performed poorly using both the CIR and colour imagery. LAI estimation using the gap fraction derived from f_c as determined by these three algorithms was not satisfactory (figure 2). The Pearson correlation of predicted vs field-measured LAI was very weak and statistically not significant ($p > 0.05$) in all cases. Only for the PCA technique was the predicted LAI within a similar range to the measured LAI. Higher LAI (>4.5) values were generally underestimated using all three algorithms, indicating a saturation effect where extracted fractional cover levels off while LAI continues to increase. As demonstrated in figure 2 and later in table 1, the three methods do produce similar trends and inter-correlations in estimated LAI. For example, for the colour imagery, the mean predicted LAI from the maximum likelihood, object-oriented and PCA techniques were 3.6, 3.4 and 3.4, respectively, and for the CIR image they were 5.6, 2.5 and 3.8, respectively.

The linear regression relationships between predicted LAI from NDVI and field-measured LAI are shown in figure 3. The relationship was stronger and the predicted

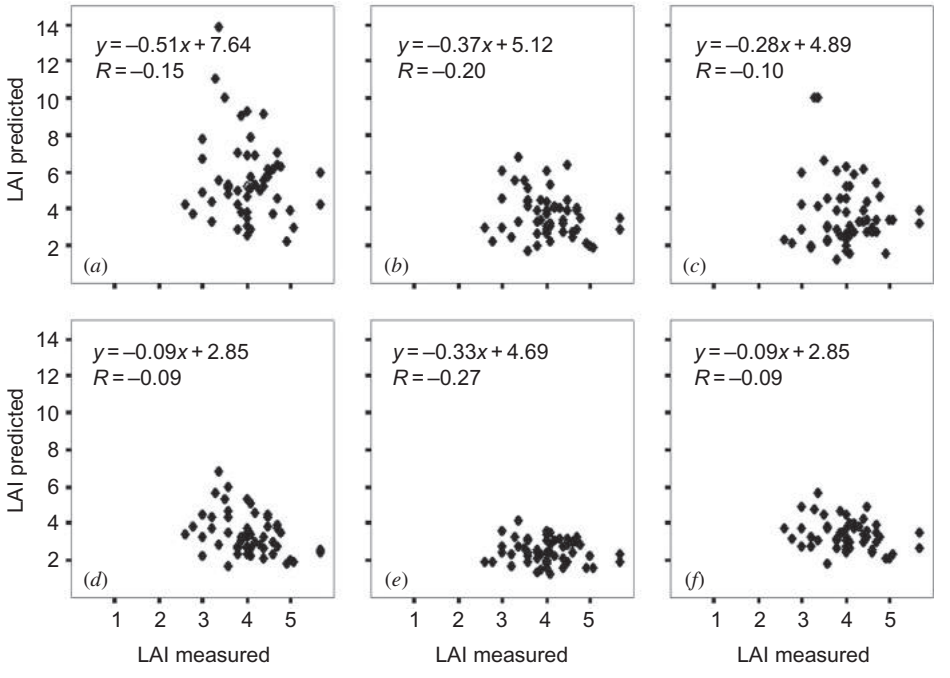

Figure 2. Relationship between *in situ* and predicted LAI using the gap fraction derived from: (*a*) CIR image using maximum likelihood classification; (*b*) colour image using maximum likelihood classification; (*c*) CIR image using object-oriented classification; (*d*) colour image using object-oriented classification; (*e*) CIR image using principal component analysis; and (*f*) colour image using principal component analysis.

Table 1. Pearson correlation matrix of LAI as estimated for the ground plots using the different gap extraction procedures.

	LAI[a]	LAI[b]	LAI[c]	LAI[d]	LAI[e]	LAI[f]	LAI[g]	LAI[h]	LAI[i]
LAI[a]	1								
LAI[b]	0.67**	1							
LAI[c]	0.76**	0.56**	1						
LAI[d]	0.55**	0.90**	0.45**	1					
LAI[e]	0.89**	0.76**	0.71**	0.60**	1				
LAI[f]	0.57**	0.67**	0.47**	0.64**	0.49**	1			
LAI[g]	–0.28*	–0.38**	–0.32*	–0.31*	–0.42**	0.12	1		
LAI[h]	–0.17	–0.07	–0.42**	0.12	–0.14	0.22	–0.01	1	
LAI[i]	–0.03	0.09	–0.01	0.19	–0.32*	–0.31*	–0.28*	0.60**	1

Notes: **Correlation is significant at the 0.01 level (two-tailed) and *correlation is significant at the 0.05 level (two-tailed).
LAI derived from: [a]colour image using maximum likelihood classification; [b]CIR image using maximum likelihood classification; [c]colour image using object-oriented classification; [d]CIR image using object-oriented classification; [e]colour image using principal component analysis; [f]CIR image using principal component analysis; [g]NDVI as background and saturated value calculated from plot subscene; [h]NDVI as background and saturated value calculated from 1% cut-off bounds from each mosaic separately; and [i]NDVI as background and saturated value calculated from 1% cut-off bounds from both mosaics combined.

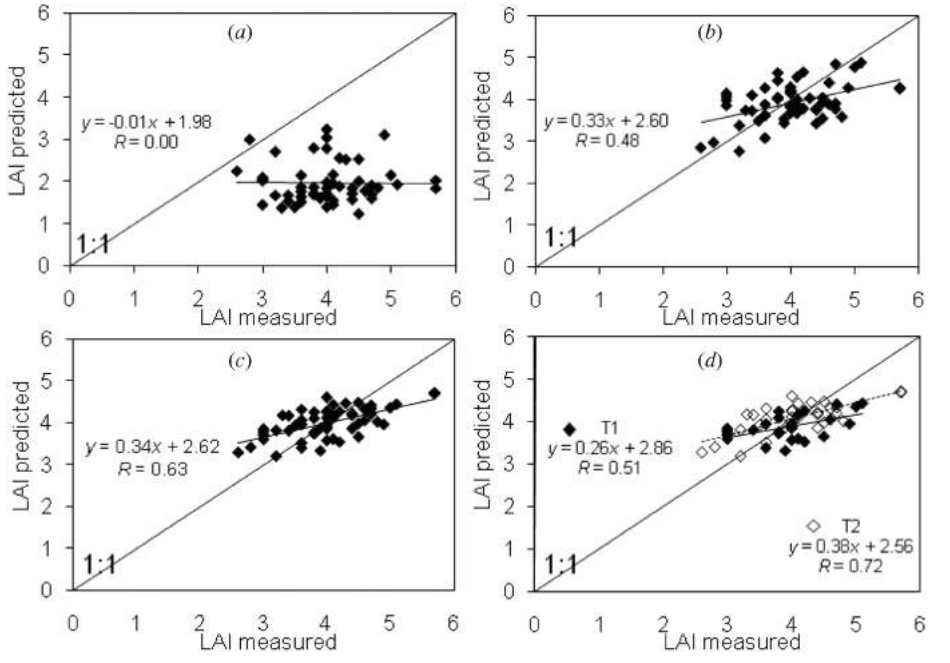

Figure 3. Relationship between *in situ* and predicted LAI using NDVI as the background and saturated NDVI for equation (8) computed from: (*a*) plot subscenes; (*b*) 1% cut-off bounds from each mosaic separately; (*c*) 1% cut-off bounds from both mosaics combined; and (*d*) the same as '(*c*)' but the LAI is plotted per transect.

LAI error was lower than for the classification and PCA procedures. From tests of the three procedures to compute background and saturated NDVI, LAI prediction was worst when they were computed from plot subscenes (figure 3(*a*)), better when computed from each transect mosaic separately (figure 3(*b*)) and best when computed from the combined histogram of both mosaics (figure 3(*c*)). This demonstrates that the saturation and background NDVI values are critical to LAI prediction using this inversion technique. The range of ground-measured LAI was between 2.6 and 5.7, whereas the range of predicted LAI using the background and saturated NDVI from both mosaics combined was between 3.2 and 4.7. A Pearson correlation (R) of 0.63 between predicted and ground-based LAI was achieved compared with correlations as low as 0.00 when background and saturated NDVI values were computed from the plot subscenes.

In figure 3(*a*) the scatterplot is similar to those for LAI predicted from the classification procedures (figure 2). In both figures 2 and 3 the basic assumption is that there is at least one 'pure' pixel or class of canopy or gap. However, for plot subscenes, this may not be true. When NDVI background and saturation values were determined from data covering a larger extent, such as a full transect mosaic, the relationship improved. The Pearson correlation was 0.51 and 0.72 for T1 and T2, respectively, when the correlation was computed for each mosaic (transect) separately (figure 3(*d*)).

The main premise of LAI inversion, particularly from the classification procedures, was that the complement of fractional vegetation cover is equal to the mono-directional gap fraction. Owing to the denseness of most of the forest, these

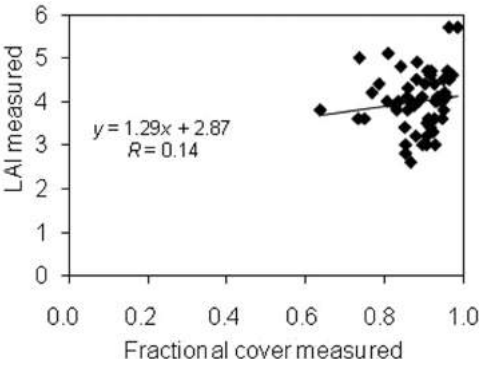

Figure 4. The relationship between LAI and fractional canopy cover as estimated *in situ* from hemispherical photography.

procedures generally performed poorly. This is evident in the poor relationship between ground-based LAI and fractional vegetation cover ($R = 0.12$, $p > 0.4$; figure 4). Additional analysis of relationships of different NDVI statistics with measured and predicted LAI (saturated and background NDVI from both mosaics combined) was also conducted using plot data and data generated from grids to determine if there was another potential variable which could be included in the inversion algorithms (figure 5). As demonstrated in figure 5, the NDVI maximum within the plot or a given grid cell shows a slight correlation with measured LAI. An increasing trend of NDVI maximum was observed with increasing LAI, particularly at low LAI, but saturation is evident for LAI values above 2. The NDVI minimum of the inversion regular grids shows a strong relation with predicted LAI. NDVI range and standard deviation (STD), the latter a first-order image texture measure, show a decreasing trend compared with predicted LAI (figure 5(*a*) and (*b*)).

Table 1 presents the correlation matrix of LAI predictions using all the algorithms for the ground plot locations. LAI predicted from classification procedures and PCA are highly correlated ($p < 0.01$), as can be seen in the scatter plot (figure 2). However, LAI predicted from the three types of NDVI analysis are only weakly related to LAI derived from the classification and PCA techniques. In addition, correlations are weak among LAI predicted from the three types of NDVI analysis except for the pair of transect-based (separately and combined) NDVI background and saturation value calculations.

All accuracy assessments showed that the LAI inversion algorithm based on NDVI using background and saturated values from the combined histogram of both mosaics was the best (table 2). Its Pearson correlation with ground-measured LAI was 0.63, the RMSE of predicted LAI was 0.5 and the OAA was 87%, which is slightly higher than the same algorithm deriving NDVI background and saturated values from the two mosaics separately. The mean predicted LAI from this algorithm was 4, which is very close to the ground-measured mean of 4.03 and slightly higher than the second best algorithm (3.91). Based on these results, this algorithm was selected for mapping LAI throughout the image data coverage.

Besides the analytical assessments presented above, visual assessment of the spatial distribution of predicted LAI was conducted. Figure 6 shows that the spatial distribution of LAI matches closely the density of colour and tone in the CIR image,

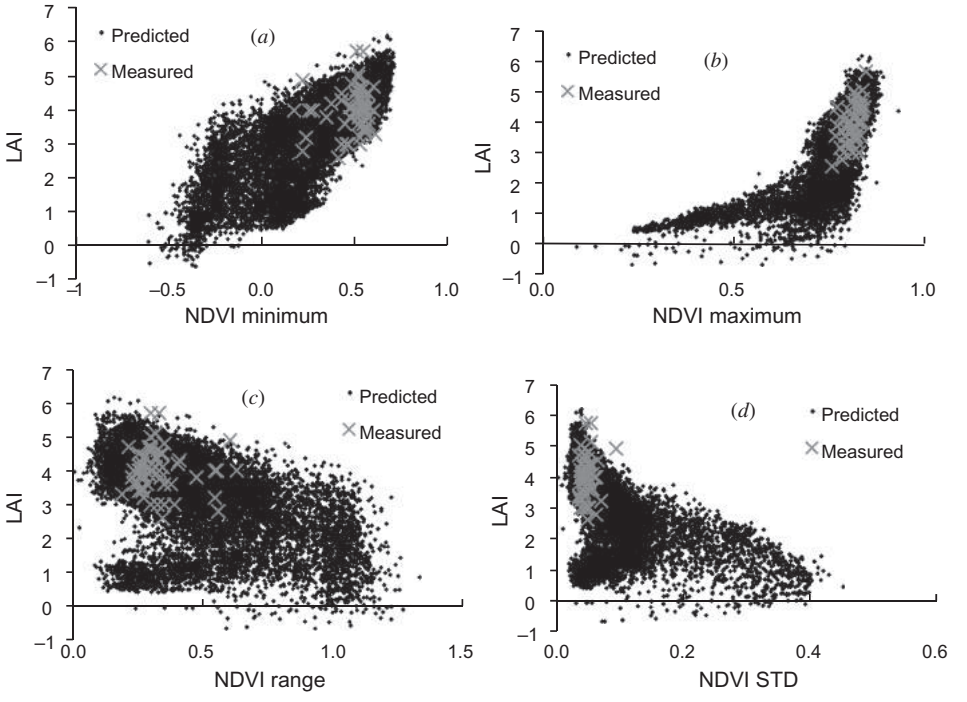

Figure 5. Relationship of predicted and measured LAI with: (*a*) NDVI minimum; (*b*) NDVI maximum; (*c*) NDVI range; and (*d*) NDVI standard deviation (STD).

Table 2. Accuracy and effectiveness assessment of LAI as estimated from different gap extraction procedures.

	LAI^a	LAI^b	LAI^c	LAI^d	LAI^e	LAI^f	LAI^g	LAI^h	LAI^i
R	–0.20	–0.15	–0.35	–0.10	–0.27	–0.09	0.00	0.48	0.63
OAA(%)	61.65	28.53	60.01	49.75	66.71	54.80	44.26	84.91	87.09
RMSE	1.53	2.85	1.60	2.01	1.33	1.81	2.23	0.60	0.52

Notes: *R* = Pearson correlation coefficient, OAA = overall average accuracy and RMSE = root mean square error.
LAI derived from: [a]colour image using maximum likelihood classification; [b]CIR image using maximum likelihood classification; [c]colour image using object-oriented classification; [d]CIR image using object-oriented classification; [e]colour image using principal component analysis; [f]CIR image using principal component analysis; [g]NDVI as background and saturated value calculated from plot subscene; [h]NDVI as background and saturated value calculated from 1% cut-off bounds from each mosaic separately; and [i] NDVI as background and saturated value calculated from 1% cut-off bounds from both mosaics combined.

both being indicative of vegetation abundance. Some mixed pixels near water, roads, built-up areas and agricultural fields resulted in low LAI estimates.

4. Discussion and conclusions

In this study, a traditional maximum likelihood classification, an object-oriented classification, PCA and NDVI-based techniques were applied to high-resolution

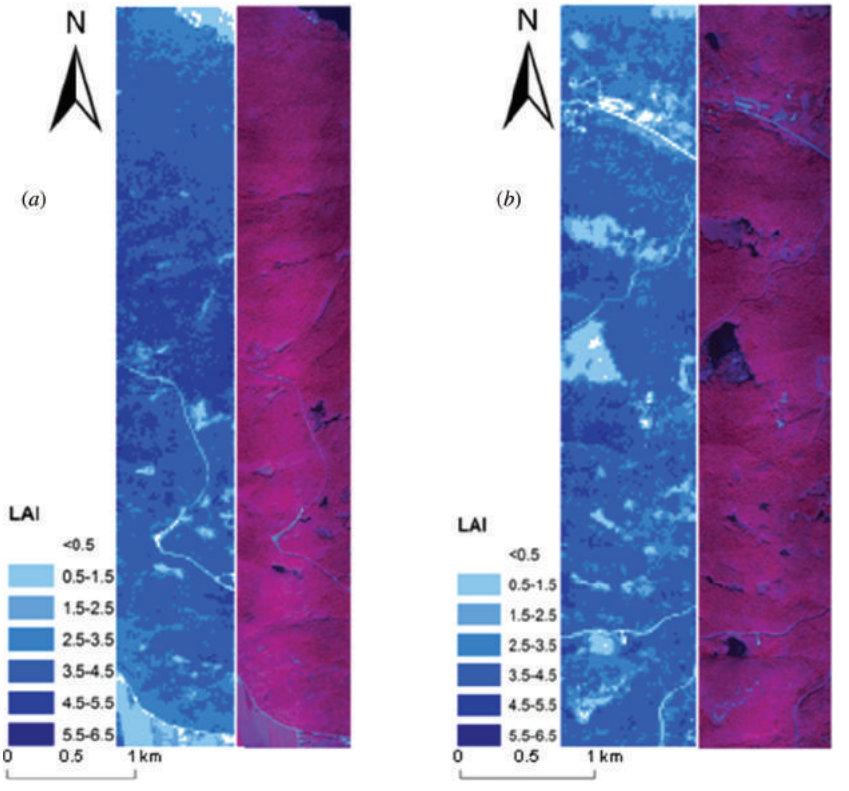

Figure 6. The LAI map (left) and CIR image mosaic (right) for: (*a*) transect two, and (*b*) transect one. LAI was estimated using the NDVI inversion algorithm (background and saturated NDVI computed from the 1% cut-off bounds of the combined NDVI histogram of both mosaics). The nominal pixel size of the LAI map and CIR image is 20 m and 60 cm, respectively.

colour and CIR airborne imagery to derive the fractional vegetation cover. It was then used to derive the gap fraction for LAI estimation. We presumed that LAI estimation from remotely sensed images can be improved by taking advantage of the existing light extinction model for forest canopies and using vegetation indices and other image-driven parameters from high spatial resolution imagery.

Fractional vegetation cover mapping using maximum likelihood and object-oriented classification methods yielded unsatisfactory results when converted to gap fraction for LAI inversion. In this study, estimation of fractional vegetation cover was dependent on accurate extraction of 'pure' canopy and gap pixels, particularly for the maximum likelihood classification technique. However, classification is usually based on image–class relationships that are empirically determined for each image using a training process. These relationships change across the mosaicked imagery producing inconsistent signatures of shadow, canopy or soil background due to the heterogeneity of the forested areas. These differences were deemed to be greater than differences in brightness caused by mosaicking several scenes as the between-scene signal difference was minimal due to the use of a narrow angle of view centred on nadir. It is also expected that the bias introduced by classifying each scene prior to mosaicking would

be larger due to subjective selection of training samples for the generation of separate class signatures for each scene. The object-oriented classification had the advantage of incorporation of more features (both spectral and spatial) with the combination of feature space optimization and nearest-neighbour classification. Image segmentation into discrete objects before classification did eliminate the 'salt and pepper' effect common in pixel-based classification of very-high-resolution images; however, many small gaps were merged with canopy (figure 7(*e*)). A single scale factor could not be found that would maintain small gap objects while segmenting larger crown objects and crown clusters. It should be noted that object-oriented classification has proven to be better than traditional pixel-based classification in other studies of land cover classification at a landscape scale (e.g. Herold *et al.* 2003, Laliberte *et al.* 2004), but in this study, where small detailed shadow objects were critical, such segmentation and classification proved difficult. In future work, multi-scale segmentation will be explored to create a hierarchical classification of small objects (gaps, foliage, etc.) up through to larger gaps and crowns for low to moderate f_c vegetation.

PCA has been frequently used with multi-dimensional remote sensing data due to its capacity of representing the total variance of a data set in a reduced number of orthogonal variables. Here, PCA was applied to extract the maximum variation in the first principal component in order to derive the fractional vegetation cover through a threshold technique in each pixel at the sub-pixel level. The first principal component corresponded mostly to overall brightness information showing a gradient related to vegetation abundance over a range between very dark pixels representing shadow and water and very light pixels representing roads and other artificial features (figure 7(*a*) and (*c*)). We supposed that through the thresholding of the brightness response, the sub-pixel vegetation and non-vegetation fractions could be determined. The results, however, showed that the PCA approach was not suitable to retrieve LAI for this data set. This is in contrast to a few other studies that have used PCA for LAI estimation directly or indirectly with better success (Hu *et al.* 2004, Lee *et al.* 2004).

The strong correlations ($R > 0.5$) obtained among the LAI values derived from the PCA, maximum likelihood and object-oriented classification methods from both colour and CIR images indicate the consistency of these methods. There is therefore no very strong reason to prefer one of these methods to the other for fractional cover extraction and LAI estimation. The primary factor contributing to the poor performance of LAI inversion based on these three procedures is the denseness of the forest that is also illustrated in the low correlation of fractional canopy cover and LAI from

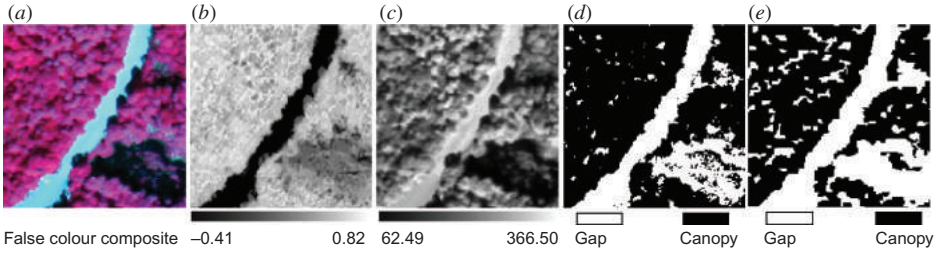

Figure 7. An example of a representative area of 100 m by 100 m showing dense forest canopy, shadow, wetland (lower right) and road. The (*a*) CIR image was used to derive, (*b*) NDVI, (*c*) PCA (DN in 32 Bit), (*d*) maximum likelihood and (*e*) object-oriented classification results.

ground measurements (figure 4). Nevertheless, a previous study has shown strong dependency of fractional vegetation cover with LAI (Carlson and Ripley 1997) in low forest cover areas and in the absence of bare soil patches.

Although there were discrepancies among the LAI estimates from PCA and the two classification methods (figure 2), they indicate well the fractional area covered by green vegetation, unlike NDVI, which is strongly related to the optical thickness of the vegetation canopy because of the high contrast of canopy and non-canopy NIR and red reflectances (Richardson and Wiegand 1977, Goel 1988, Carlson and Ripley 1997, Gutman and Ignatov 1998). The PCA is done by finding a new set of orthogonal axes that have their origin at the data mean and that are rotated so that the data variance is maximized. Therefore, unlike the NDVI, the first principal component used in this study shows features that are consistent (most highly correlated) among the data set such as intra-class properties, which are not intrinsically related to the optical thickness of the photosynthetic biomass (figure 7). In such cases, particularly with classification methods where small gaps are non-detectable even with the use of high-resolution imagery (figure 7(*d*) and (*e*)), the exponential extinction of light transmission under a forest canopy is not adequately represented using Beer–Lambert's law (Bréda 2003). If the classification algorithms were applied to imagery acquired from two or more directions (view angles), the canopy geometry including leaf angle orientation, shadows and the radiometric component of the background and canopy structures could have been derived for the gap fraction. In such a way, the exponential extinction of light in the forest canopy would have been described by the extinction coefficient (Bréda 2003). However, precisely separating the radiometric component into sunlit and shaded background and sunlit and shaded canopy is not feasible using only a few spectral bands and the classification methods applied in this study. As shown in figure 7(*c*), the PCA analysis, however, has considerable potential for extraction of the sunlit and shaded components of background and canopy, as well as shadow geometries, in a manner analogous to spectral unmixing, due to the very high-resolution of the imagery. Sunlit and shaded components of background and canopy may show correlated responses in each band, resulting in less discrepancy in image future such as NDVI. PCA, however, reveals the internal structure in its most informative way, which explains the variance of the data by shifting the axes that show strong correlation using all bands considered (see NDVI and PCA images in figure 7(*b*) and (*c*); Plaza and Chang 2007). As shown in figure 7(*d*) and (*e*), the gap size and distribution which control the physical basis for LAI estimation may not be adequately exploited with classification methods. A previous study conducted in a mixed coniferous–deciduous boreal forest with very-high-resolution CIR imagery (25 cm) and lower ground-measured LAI values compared with this study also found that shadow fraction was a poor predictor of LAI (Seed and King 2003). We acknowledge at this stage that the classification methods using broad band multispectral imagery are not feasible and practical for robust extraction of the gap fraction for LAI estimation, particularly for densely vegetated temperate hardwood ecosystems.

In addition to the aforementioned limitations explained in this study, the LAI estimated from the ground measurements and the PCA and classification methods may not be directly comparable with LAI estimated from the NDVI-based method. The NDVI responds to photosynthetic biomass reflectance in the NIR and red bands and indicates the 'green' LAI, whereas the LAI estimated from other methods represents the amount of foliage, branches and stems as opaque structures. These

characteristics might be incorporated in future studies to adequately explain the light regime under the forest canopy and the canopy radiation interception. NDVI is capable of partial self-cancelation of interfering effects (e.g. bi-directional, atmospheric and shadow effects; figure 7(*b*)) by mathematically normalizing the NIR and red differences for each pixel (Gutman and Ignatov 1998). In addition, NDVI is directly proportional to the photosynthetic status of the vegetation (figure 7(*a*) and (*b*)). On the other hand, PCA clearly shows the shadow geometry and the shadow and sunlit components of background and canopy elements (figure 7(*c*)), and therefore these are treated separately in equation (4) for f_c estimation. Further, the LAI estimates obtained from PCA analysis of both colour and CIR imagery were within the range of ground-based LAI (figure 2(*e*) and (*f*)). Therefore, future research will look to integrate the PCA and NDVI-based LAI estimation methods to represent both the photosynthetic and structural aspects of the forest canopy over a wider range of fractional cover and LAI. This is particularly useful in temperate forests, where the shaded LAI fraction is comparably larger and important in upscaling photosynthesis models (Liu *et al*. 2002).

The result achieved using the NDVI inversion appears to be better than what most authors tend to achieve using coarser-resolution satellite images (Baret *et al*. 1995, Gutman and Ignatov 1998, Jiang *et al*. 2007, Tang *et al*. 2007). The use of high-spatial-resolution imagery may improve the accuracy of LAI inversion to a certain extent, but it does not reduce the uncertainty in NDVI caused by the variation of understorey and soil background. Higher accuracy of LAI inversion from NDVI can be achieved by adjusting the saturation and background NDVI values according to the observed data if *in situ* observations are available, taking into account the understorey effect. This practical and parameter-independent LAI inversion algorithm can be greatly improved along with the traditional methods through further research.

Compared with the other methods, the best result in this study was obtained using the NDVI-based inversion algorithm ($R = 0.63$, RMSE $= 0.52$), while the classification and PCA methods were not effective. LAI estimated from the NDVI method was then used to produce LAI maps of the study area, which showed that the spatial distribution of LAI over the two transects matched that interpreted from the CIR imagery. These results show that further testing of this procedure as an alternative approach for LAI retrieval from remote sensing datasets is warranted. In future research, the influence of shadow geometry will be investigated as it changes with view angle, sun angle and topography. Within-crown shadows from mutual shading of adjacent branches or trees are also problematic because they reduce NDVI independently of LAI at that location. This leads to increased noise in the NDVI values used to estimate LAI in equation (9). Further research is also required to determine the effects of variations in the extinction coefficient and soil background for the NDVI-based method and determine the correction factor for converting f_c to the gap fraction for equation (9) through interactive regression analysis. This work is currently underway using independent datasets and a canopy radiative transfer model. This will enable development of a portable and efficient large-scale LAI inversion model.

Acknowledgements

The research was funded by the Academy of Finland through the TAITATOO-project and personal grant to PP (120190), and by the Natural Sciences and Engineering Research Council of Canada funding to DK. We are very grateful to Jon Pasher, PhD candidate at Carleton University, for the airborne imagery

acquisition. A.G. and P.P. are also grateful for the working infrastructure and environment provided by the Geomatics and Landscape Ecology Laboratory (GLEL) and the Department of Geography and Environmental Studies of Carleton University during the fieldwork stay in August 2007. A.G. is financed partly by CIMO, Department of Geography of University of Helsinki, and the Finnish Graduate School of Geography.

References

Asner, G.P., Scurlock, J.M.O. and Hicke, J.A., 2003, Global synthesis of leaf area index observations: Implications for ecological and remote sensing studies. *Global Ecology and Biogeography*, **12**, pp. 191–205.

Baret, F., Clevers, J.G.P.W. and Steven, M.D., 1995, The robustness of canopy gap fraction estimates from red and near-infrared reflectances: a comparison of approaches. *Remote Sensing of Environment*, **54**, pp. 141–151.

Berterretche, M., Hudak, A.T., Cohen, W.B., Maierspergera, T.K., Gower, S.T. and Dungan, J., 2005, Comparison of regression and geostatistical methods for mapping Leaf Area Index (LAI) with Landsat ETM+ data over a boreal forest. *Remote Sensing of Environment*, **96**, pp. 49–61.

Bréda, N.J.J., 2003, Ground-based measurements of leaf area index: a review of methods, instruments and current controversies. *Journal of Experimental Botany*, **54**, pp. 2403–2417.

Carlson, T.N. and Ripley, D.A., 1997, On the relation between NDVI, fractional vegetation cover, and leaf area index. *Remote Sensing of Environment*, **62**, pp. 241–252.

Carpenter, G.A., Gopal, S., Macomber, S., Martens, S. and Woodcock, C.E., 1999, A neural network method for mixture estimation for vegetation mapping. *Remote Sensing of Environment*, **70**, pp. 138–152.

Demarez, V., Duthoit, S., Baret, F., Weiss M. and Dedieu, G., 2008, Estimation of leaf area and clumping indexes of crops with hemispherical photographs. *Agricultural and Forest Meteorology*, **148**, pp. 644–655.

Goel, N.S., 1988, Models of vegetation canopy reflectance and their use in estimation of biophysical parameters from reflectance data. *Remote Sensing Reviews*, **4**, pp. 1–212.

Gong, P., Pu, R., Biging, G.S. and Larrieu, M.R., 2003, Estimation of forest leaf area index using vegetation indices derived from hyperion hyperspectral data. *IEEE Transactions on Geoscience and Remote Sensing*, **41**, pp. 1355–1362.

Gonsamo, A. and Pellikka, P., 2008, Methodology comparison for slope correction in canopy leaf area index estimation using hemispherical photography. *Forest Ecology and Management*, **256**, pp. 749–759.

Gutman, A. and Ignatov, G., 1998, The derivation of the green vegetation fraction from NOAA/ AVHRR data for use in numerical weather prediction models. *International Journal of Remote Sensing*, **19**, pp. 1533–1543.

Herold, M., Liu, X. and Clarke, K.C., 2003, Spatial metrics and image texture for mapping urban land use. *Photogrammetric Engineering and Remote Sensing*, **69**, pp. 991–1001.

Hu, B., Miller, J.R., Chen, J.M. and Hollinger, A., 2004, Retrieval of the canopy leaf area index in the BOREAS flux tower sites using linear spectral mixture analysis. *Remote Sensing of Environment*, **89**, pp. 176–188.

Jensen, J.R., 1996, *Introductory Digital Image Processing: A Remote Sensing Perspective* (Englewood Cliffs, NJ: Prentice-Hall).

Jiang, Z., Huete, A.R., Chen, J., Chen, Y., Li, J., Yan, G. and Zhang, X., 2007, Analysis of NDVI and scaled difference vegetation index retrievals of vegetation fraction. *Remote Sensing of Environment*, **101**, pp. 366–378.

Jonckheere, I., Fleck, S., Nackaerts, K., Muysa, B., Coppin, P., Weiss, M. and Baret, F., 2004, Review of methods for *in situ* leaf area index determination Part I. Theories, sensors and hemispherical photography. *Agricultural and Forest Meteorology*, **121**, pp. 19–35.

King, D.J., Olthof, I., Pellikka, P., Seed, E.D. and Butson, C., 2005, Modelling and mapping forest ice storm damage using remote sensing and environmental data. *Natural Hazards, Special Issue on Remote Sensing*, **35**, pp. 321–342.

Laliberte, A.S., Rango, A., Havstad, K.M., Paris, J.F., Beck, R.F., McNeely, R. and Gonzalez, A.L., 2004, Object-oriented image analysis for mapping shrub encroachment from 1937–2003 in southern New Mexico. *Remote Sensing of Environment*, **93**, pp. 198–210.

Leblanc, S.G., Chen, J.M. and Cihlar, J., 1997, NDVI directionality in boreal forests: a model interpretation of measurements. *Canadian Journal of Remote Sensing*, **23**, pp. 369–380.

Leblanc, S.G., Chen, J.M., Fernandes, R., Deering, D.W. and Conley, A., 2005, Methodology comparison for canopy structure parameters extraction from digital hemispherical photography in boreal forests. *Agricultural and Forest Meteorology*, **129**, pp. 187–207.

Lee, K.-S., Cohen, W.B., Kennedy, R.E., Maiersperger, T.K. and Gower, S.T., 2004, Hyperspectral versus multispectral data for estimating leaf area index in four different biomes. *Remote Sensing of Environment*, **91**, pp. 508–520.

Lévesque, J. and King, D.J., 1999, Airborne digital camera image semivariance for evaluation of forest structural damage at an acid mine site. *Remote Sensing of Environment*, **68**, pp. 112–124.

Liu, J., Chen, J.M., Cihlar, J. and Chen, W., 2002, Remote sensing based estimation of net primary productivity over Canadian landmass. *Global Ecology and Biogeography*, **11**, pp. 115–129.

Pellikka, P., 1998, Development of correction chain for multispectral airborne video camera data for natural resource assessment. *Fennia*, **176**, pp. 1–110.

Pellikka, P., King, D.J. and Leblanc, S.G., 2000a, Quantification and reduction of bidirectional effects in deciduous forest in aerial CIR imagery using two reference land surface types. *Remote Sensing Reviews*, **19**, pp. 259–291.

Pellikka, P., Seed, E.D. and King, D.J., 2000b, Modelling deciduous forest ice storm damage using aerial CIR imagery and hemispheric photography. *Canadian Journal of Remote Sensing*, **26**, pp. 394–405.

Plaza, A. and Chang, C.-I. (Eds), 2007, *High Performance Computing in Remote Sensing*, p. 496. Computer & Information Science Series (Boca Raton, FL: Chapman & Hall/CRC Press).

Price, J.C., 1990, Using spatial context in satellite data to infer regional scale evapotranspiration. *IEEE Transactions on Geoscience and Remote Sensing*, **28**, pp. 940–948.

Richardson, A.J. and Wiegand, C.L., 1977, Distinguishing vegetation from soil background information. *Photogrammetric Engineering and Remote Sensing*, **43**, pp. 1541–1552.

Seed, E.D. and King, D.J., 2003, Shadow brightness and shadow fraction relations with effective leaf area index: importance of canopy closure and view angle in mixedwood boreal forest. *Canadian Journal of Remote Sensing*, **29**, pp. 324–335.

Sellers, P. J., Mintz, Y., Sud, Y.C. and Dalcher, A., 1986, A simple biosphere model (SiB) for use within general circulation models. *Journal of the Atmospheric Sciences*, **43**, pp. 505–531.

Sprintsin, M., Karnieli, A., Berliner, P., Rotenberg, E., Yakir, D. and Cohen, S., 2007, The effect of spatial resolution on the accuracy of leaf area index estimation for a forest planted in the desert transition zone. *Remote Sensing of Environment*, **109**, pp. 416–428.

Tang, S., Chen, J.M., Zhu, Q., Li, X., Chen, M., Sun, R., Zhou, Y., Deng, F. and Xie, D., 2007, LAI inversion algorithm based on directional reflectance kernels. *Journal of Environmental Management*, **85**, pp. 638–648.

Turner, D.P., Kennedy, R.E., Cohen, W.B., Fassnacht, K.S. and Briggs, J.M., 1999, Relationships between leaf area index and Landsat TM spectral vegetation indices across three temperate zone sites. *Remote Sensing of Environment*, **70**, pp. 52–68.

WATSON, D.J., 1947, Comparative physiological studies in growth of field crops. I. Variation in net assimilation rate and leaf area between species and varieties, and within and between years. *Annatomy and Botany*, **11**, pp. 41–76.

WULDER, M.A., FRANKLIN, S.E. and LAVIGNE, M.B., 1996, High spatial resolution optical image texture for improved estimation of forest stand leaf area index. *Canadian Journal of Remote Sensing*, **22**, pp. 441–449.

WULDER, M.A., LEDREW, E.F., FRANKLIN, S.E. and LAVIGNE, M.B., 1998, Aerial image texture information in the estimation of northern deciduous and mixed wood forest leaf area index (LAI). *Remote Sensing of Environment*, **64**, pp. 64–76.

XIAO, J. and MOODY, A., 2005, A comparison of methods for estimating fractional green vegetation cover within a desert-to-upland transition zone in central New Mexico, USA. *Remote Sensing of Environment*, **98**, pp. 237–250.